JMEPEG (2012) 21:2328–2339
DOI: 10.1007/s11665-012-0205-4

1059-9495/$19.00

Parametric Study of Friction Stir Processing of Magnesium-Based AE42 Alloy

H.S. Arora, H. Singh, and B.K. Dhindaw

(Submitted November 2, 2011; in revised form February 14, 2012)

Friction stir processing (FSP) is one of the severe plastic deformation processes which can significantly affect the material properties. The friction stir processed (FSPed) zone is extremely sensitive to the FSP parameters. The main aim of the current investigation is to analyze the simultaneous influence of the major FSP parameters on the mechanical behavior of a magnesium-based AE42 alloy. In this investigation, Taguchi's experimental design approach was utilized to determine the optimized set of investigated FSP parameters for processing the AE42 alloy. Hardness of the FSPed specimens was considered as the output response of the experimental design. Cooling temperature during FSP, FSP tool rotational speed, and number of FSP passes were found to be the most influential FSP parameters in the current investigation. A nonlinear regression equation for the output response and the FSP process parameters was also developed using MINITAB 16 software. The developed equation was found to accurately predict the output response of the FSPed AE42 alloy

Keywords friction stir processing, hardness, magnesium alloy

1. Introduction

Magnesium alloys, the lightest among structural materials, have become attractive candidate for applications in automotive, aerospace, audio, and electronic industries (Ref 1-6). The main problem which limits the extensive utilization of magnesium and its alloys for different applications is their poor strength and lower elastic modulus (Ref 7, 8). Extensive research has been done on the alloy development to overcome these persistent problems. One of the most promising alloys developed was AE42 alloy, which has a considerable amount of rare earth elements (Ref 9). In the past decade, severe plastic deformation (SPD) approaches were applied to the grain refinement of Mg alloys on bulk materials. However, in most of the cases, the grain size of the final refined structure is in the micrometer or sub-micrometer range (Ref 10). It has been reported that a relatively new processing technique known as friction stir processing (FSP) can refine the microstructure of alloys by intense plastic deformation at working temperature (Ref 11-15). After the successful advent of FSP, the application arena of this technology has been growing rapidly. Some of its most recent applications involve surface modifications, enhancement of surface, and bulk properties and generation of in-situ and ex-situ nanocomposites in number of aluminum- and magnesium-based alloys. Several investigators, such as Freeney and Mishra (Ref 16), Ni et al. (Ref 17), Cavaliere and DeMarco (Ref 18), had demonstrated the enhancement of bulk properties such as tensile strength and fatigue strength of the FSPed magnesium alloys. In one of the recent investigations by Yuan et al. (Ref 19), the effect of FSP-induced texture on anisotropy in mechanical behavior was discussed. An extensive review on FSP by Mishra and Mahoney (Ref 20) covers wide aspects of this technology such as enhanced room temperature superplastic forming, modification of fusion welds by FSP for increased fatigue resistance, influence of FSP on the corrosion resistance and surface composite fabrication, etc.

It is well known that the FS processed zone is extremely sensitive to the processing parameters. The material flow behavior is predominantly influenced by the FSP tool profile, tool dimensions, and process variables (Ref 21). Some studies have been conducted to determine the process parameters that influence the metallurgical and mechanical characterization of FSPed specimen. Elangovan et al. (Ref 22) analyzed the influence of tool pin profile and axial force on the formation of FSP zone in AA6061 aluminum alloy. The role of process variables in the FSP of cast aluminum A319 alloy was investigated by Karthikeyan et al. (Ref 23) where processing was done at three different traverse feed rates and five tool rotational speeds. Chen et al. (Ref 24) investigated the effect of processing parameters on microstructure and mechanical properties of an Al-$Al_{11}Ce_3$-Al_2O_3 in-situ composite produced by FSP. In all such investigations, analysis was done by varying a single parameter at a time and keeping all other parameters at fixed levels. However, in a real working environment, the behavior of a particular parameter is influenced by the level of other parameters as well because of their mutual interactions with each other. Therefore, in an investigation which involves variation of a single parameter at a time, the visualization of impact of various factors becomes impossible. In comparison to the conventional methodology of varying single parameter at a time, the design of experiments (DOEs) technique provides the possibility of simultaneous variation of all the influencing

H.S. Arora and **H. Singh**, School of Mechanical, Material and Energy Engineering, Indian Institute of Technology Ropar, Rupnagar, 140001 Punjab, India; and **B.K. Dhindaw**, School of Materials & Mineral Resources, Universiti Sains Malaysia, Engineering Campus, 14300 Nibong Tebal, Pulau Penang, Malaysia. Contact e-mails: harpreetsingh@iitrpr.ac.in and hn97@rediffmail.com.

parameters. The DOE technique has the capability to systematically evaluate the significance of each parameter as well as the interaction level between the factors. Further, the full factorial experimental design approach of DOE involves large number of experiments to be performed to reach at a conclusion which results in material wastage, loss of time and effort. On the other hand, using an experimental strategy based on Taguchi's design approach considerably reduces the number of experiments to be performed without compromising the result reliability.

The major chunk of recent investigations done on aluminum and magnesium alloys using FSP technology has focused either on the individual effect of external particle addition into the material during FSP for ex-situ composite fabrication or the sole effect of rapid cooling during FSP for microstructural control. The investigation on an alloy system which has the capability of generating in-situ particles together with the combined influence of instant cooling during FSP has not been reported so far. AE42 alloy represents one such alloy system where in-situ particles are precipitated during transformation cooling and they can be further refined by FSP. In the current investigation, Taguchi's DOE technique incorporating orthogonal arrays was utilized for the systematic evaluation of the different FSP process parameters. The output response for this investigation was selected to be hardness of the FSPed specimens. An empirical relation between hardness of the nugget region of FSPed specimen and the selected FSP process parameters was developed using nonlinear regression equation on MINITAB 16 software. The adequacy of the developed empirical relation was checked using comparison of the experimental and the predicted values and by the residual plots of the developed equation.

2. Methodology of Investigation

2.1 Identifying the Important Process Parameters

Based on literature (Ref 25-28) and the experimental results of some preliminary investigations conducted on AE42 alloy using FSP, it was concluded that the major factors that influence the strength of the material can be FSP tool rpm, tool linear speed, plunge depth of the FSP tool, cooling temperature during FSP, and number of FSP passes. These are the predominant factors that affect the highest temperature achieved during FSP along with strain rate imposed on FSPed specimen, length of exposure of the specimen to higher heat, recrystallized grain growth rate, grain size, and finally the strength of the FSPed specimen.

2.2 Evaluating the Working Limits of the Parameters

As is the normal procedure, the working limits for the above-mentioned FSP parameters were worked out from the results of trial FSP experiments conducted on the investigated alloy so that the final DOE gives the best optimal properties. The working limits of all the factors considered are given in Table 1. As shown, three levels of each investigated factor were considered. The ranges of FSP tool rpm, tool linear speed, and plunge depth have been selected as 700-900 rpm, 40-60 mm/min, and 0.25-0.35 mm, respectively. During trial experiments, it was observed that FSP of AE42 alloy within these limits produced a defect-free nugget zone whereas a defective nugget/stir zone was produced outside these parameters limits, which generally consisted of cracks and long tunnel defects in the nugget zone as shown in Fig. 1.

Table 1 Factors and levels chosen for the Taguchi's experimental design

Control factors	Levels			Units
	I	II	III	
Tool rotational speed (*A*)	700	800	900	rpm
Cooling temperature (*B*)	−10 (263)	10 (283)	30 (303)	°C (K)
Linear speed (*C*)	40	50	60	mm/min
Plunge depth (*D*)	0.25	0.3	0.35	mm
Number of passes (*E*)	1	2	3	

In some of the investigations such as by Yuan et al. (Ref 19), the formation of defect-free FSP zone has been reported at 204 mm/min and 700 rpm for AZ31 magnesium alloy which is about 3.4 times the linear speed used in the current investigation. In view of such investigations, the selected range of parameter may appear to fall within a narrow range but, however, the above mentioned range appears narrow because of large number of parameters investigated in the current study. It was observed that the range of each parameter became narrower with the increase in the number of parameters because of enhanced interaction effect between the parameters. For an illustration, in the current investigation the FSP zone was defect free at 700 rpm, 70 mm/min linear speed, and 0.3 mm plunge depth for a single pass FSP whereas for multipass FSP, the zone became defective at the same FSP parameters, which however remained defect free at 60 mm/min even for multipass FSP of AE42 alloy. This may have happened because the FSP zone became thinner after the first pass because of removal of flash and the frictional heat input in the FSP zone at 70 mm/min may fall short of than the required amount for efficient plasticization and consolidation of the material in the stir zone. Number of passes is known to be an important FSP parameter for a desired material performance through microstructural evolution and thus cannot be overlooked.

In a recent investigation by the authors (Ref 29), it was found that FSP tends to fragment the in-situ precipitate particles. This is evident from the SEM images shown in Fig. 2. The SEM image shown in Fig. 2(a) represents the base metal, transition zone, and friction stir processed (FSPed) zone of AE42 alloy subjected to FSP whereas, the SEM image shown in Fig. 2(b) shows the fragmented precipitates produced in the nugget zone of FSP AE42. The FSP process parameters such as tool rpm and number of FSP passes significantly affect the size and distribution of in-situ precipitate particles. It was observed that single pass FSP of AE42 alloy resulted in generation of in-situ precipitates with smallest particle size of the order of 200 nm which get further refined to about 50 nm during double pass FSP. It was concluded that the presence of fine in-situ precipitates contributed towards evolution of the ultra-fine grain structure through particle pinning of the fine nuclei. As an illustration, the grain size of AE42 magnesium alloy FSPed at 900 rpm and 60 mm/min linear speed with undersurface cooling was found to about 0.8 μm. In the above-mentioned investigation, the grain growth equations which take into consideration the effect of rapid cooling only were used to find out the influence of in situ particles in refining the grain

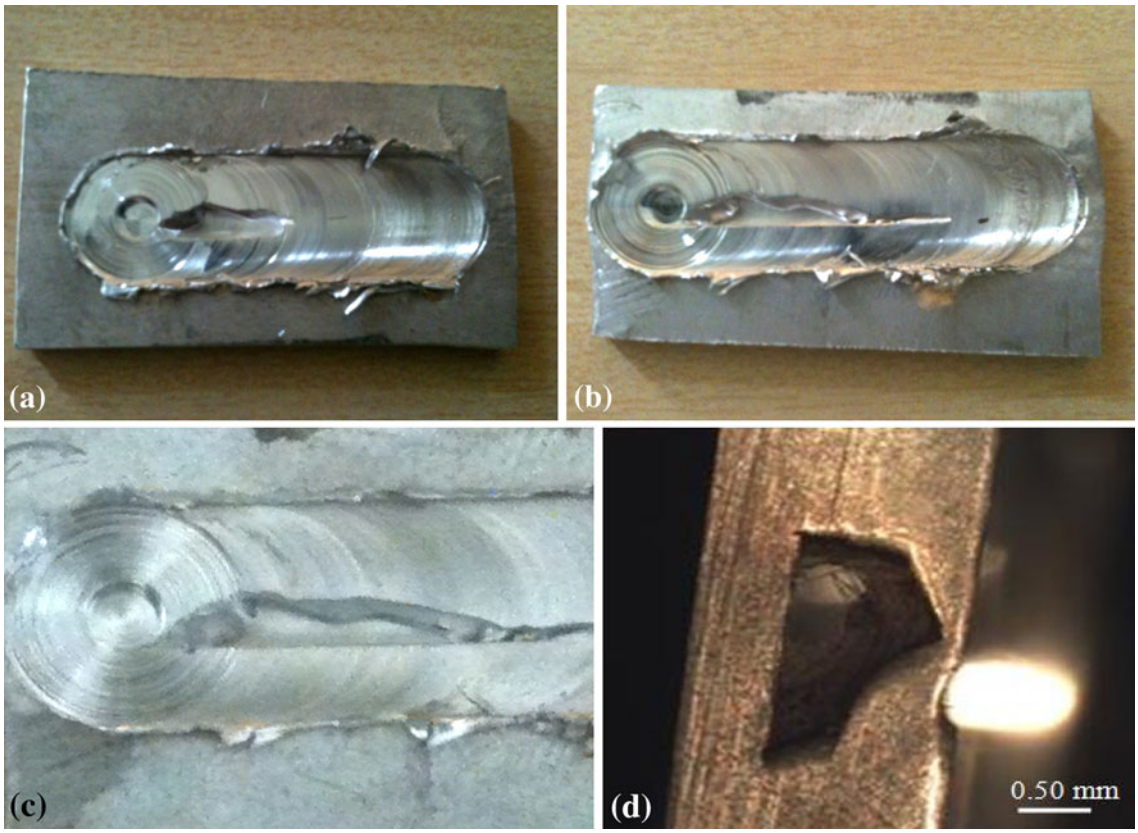

Fig. 1 Optical images showing the tunnel defect in the FSPed AE42 specimen. (a) Fabricated at 1100 rpm, 40 mm/min linear speed, 0.3 mm plunge depth, 3 FSP passes, 30 °C cooling temperature, (b) Fabricated at 900 rpm, 60 mm/min linear speed, 0.2 mm plunge depth, 1 FSP pass, 30 °C cooling temperature, and (c) enlarged view of image shown in (b) and (d). Optical image showing the cross section of the image shown in (a)

size. It was found that considering the effect of rapid cooling only, the grain size would have been 2.5 μm instead of 0.8 μm. This difference in the grain size values was attributed to the presence of fine in-situ particles which through the particle pinning phenomena resulted in the evolution of finer grain structure. The microhardness value of the as-cast AE42 alloy was found to enhance from 63 HV to 77.46 HV and to 111 HV for the single pass and double pass FSP, respectively. Thus, the range of the selected parameters should not be interpreted on individual basis for fabrication of defect-free FSP zone as their cumulative influence has to be reported for the targeted analysis in the current investigation. The cooling temperature during FSP was varied from natural cooling (~30 °C (303 K)) to −10 °C (263 K) using a chiller unit and LR grade methanol as refrigerant. The lowest temperature of −10 °C (263 K) was used because of the limitation of the available chiller unit.

2.3 Experimental Details

Rectangular specimen having dimensions 80 × 40 × 3 mm were prepared from an AE42 alloy ingot. The chemical composition of this alloy is shown in Table 2. FSP was conducted on a CNC vertical milling machine using a specially designed fixture. The details of the FSP fixture are given in Fig. 3 (Ref 29). The fixture has the configuration of a hollow rectangular box for the flow of cooled liquid so as to facilitate the undersurface cooling of the processed specimen. A cryostat cooling bath of 250 W with 8 L capacity was used to produce the rapid cooling to a temperature of −10 °C (263 K). The circulating liquid used in the cryostat bath was LR grade methanol. Polyurethane (PU) pipes with thermal insulations were used for connecting the fixture to the cryostat bath. The FSP tool was a commonly used HSS cylindrical tool without threads with 12 mm shoulder diameter, 4 mm pin diameter, and 2.7 mm pin length. In the current investigation, dry ice was initially placed in the cryostat cooling bath at the investigated cooling temperature of −10 °C (263 K) or 10 °C (283 K). As the FSP tool progressed, solidified dry ice was placed on FSPed part of the specimen just behind the tool. This process was continued until FSP tool was pulled back and cooled by dry ice instantaneously. As soon as the FSP tool was pulled back, methanol at the investigated cooling temperature was circulated to cool the specimen underneath. Cooling was done until room temperature was achieved. In the case of multi-pass FSP, FSP tool was moved over the same path, in the same direction for the second pass also. Cooling in case of multi-pass FSP was done in the second pass only.

The output response considered in this investigation was bulk hardness of the FSPed specimens. The bulk hardness testing of the FSPed specimens was done on a universal hardness testing machine of Zwick Roell make (Model no. 8187.5KV). The bulk hardness measurements were done on the polished surfaces at three different places in the nugget zone of the FSPed specimen and average of these values was reported as the sample's hardness on the Vickers scale. The hardness testing was done at 5 kg·f load for a dwell period of 10 s. Metallurgical examination of the as-cast AE42 and FSPed samples was carried out by optical microscope (Leica make).

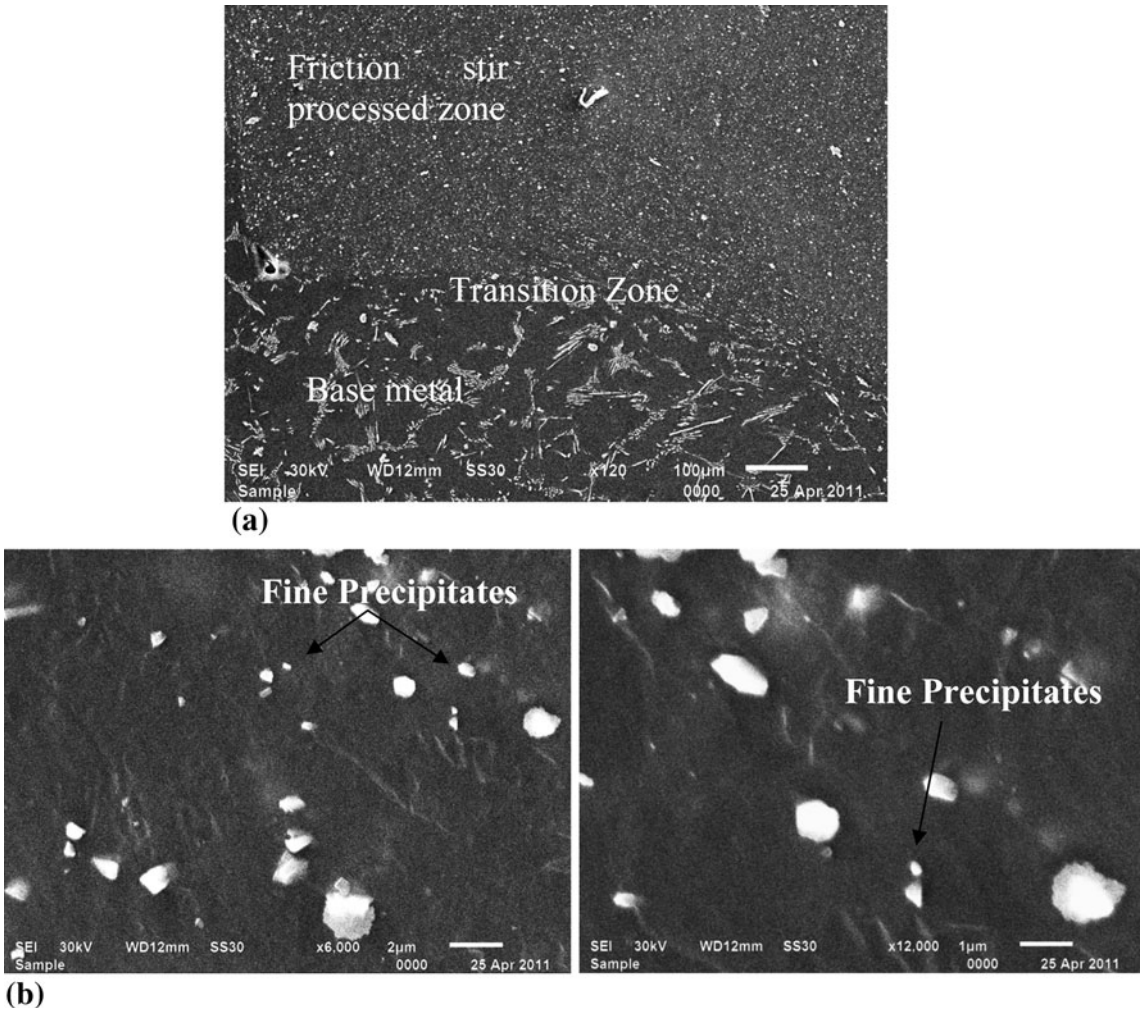

Fig. 2 SEM images showing (a) the base metal, transition zone, and the FSPed zone and (b) fragmented precipitate particles in the nugget zone of the AE42 alloy subjected to FSP (Ref 29)

Table 2 Chemical composition of AE42

Elements	Al	Ce	La	Nd	Mn	Th	Pr	Si	Zn	Mg
AE42	3.9	1.2	0.6	0.4	0.3	0.2	0.1	0.01	<0.01	Balance

2.4 Developing Experimental Design Matrix

As mentioned earlier, five factors each having three levels were used in the current investigation. The orthogonal array corresponding to five factors and three levels is L_{27}, where the subscript 27 denotes the number of experiments to be performed. The L_{27} orthogonal array is shown in Table 3. Each column in table represents a test parameter whereas each row represents a test condition which is formed by combination of different levels of the investigated parameters. Tool rpm (parameter *A*) has been assigned to 1st column, cooling temperature (parameter *B*) to 2nd column. The line graph for L_{27} array has been shown in Fig. 4. The line graph is made up of numbers, dots, and lines, where a dot and the number identifies a factor, a connecting line between two dots indicates interaction and the number assigned to the line indicates the column number in which the interaction effects will be compounded. The line graph facilitates laying out experiments with interactions. The use of line graphs can greatly reduce the time and increases the accuracy of assigning proper columns for interaction effects (Ref 30). According to this figure, the interaction factor between parameters *A* and *B* can be assigned to either 3rd or 4th column. In the current design, this is assigned to column 3. Factor *C* (linear speed) was assigned to 5th column and interaction between factors *A* and *C* ($A \times C$) to column 8, and factors *D* and *E* to column numbers 9 and 10, respectively, in accordance with the line graph. The number of experiments required using a full factorial design would have been 3^5.

Based on the output response, the Vickers hardness values, in all the 27 investigated cases, Taguchi's experimental design was analyzed on MINITAB 16 software. Signal-to-noise ratio (SN ratio), which measures the sensitivity of the quality characteristic being investigated in a controlled manner to the external influencing factors (noise factors) not under control,

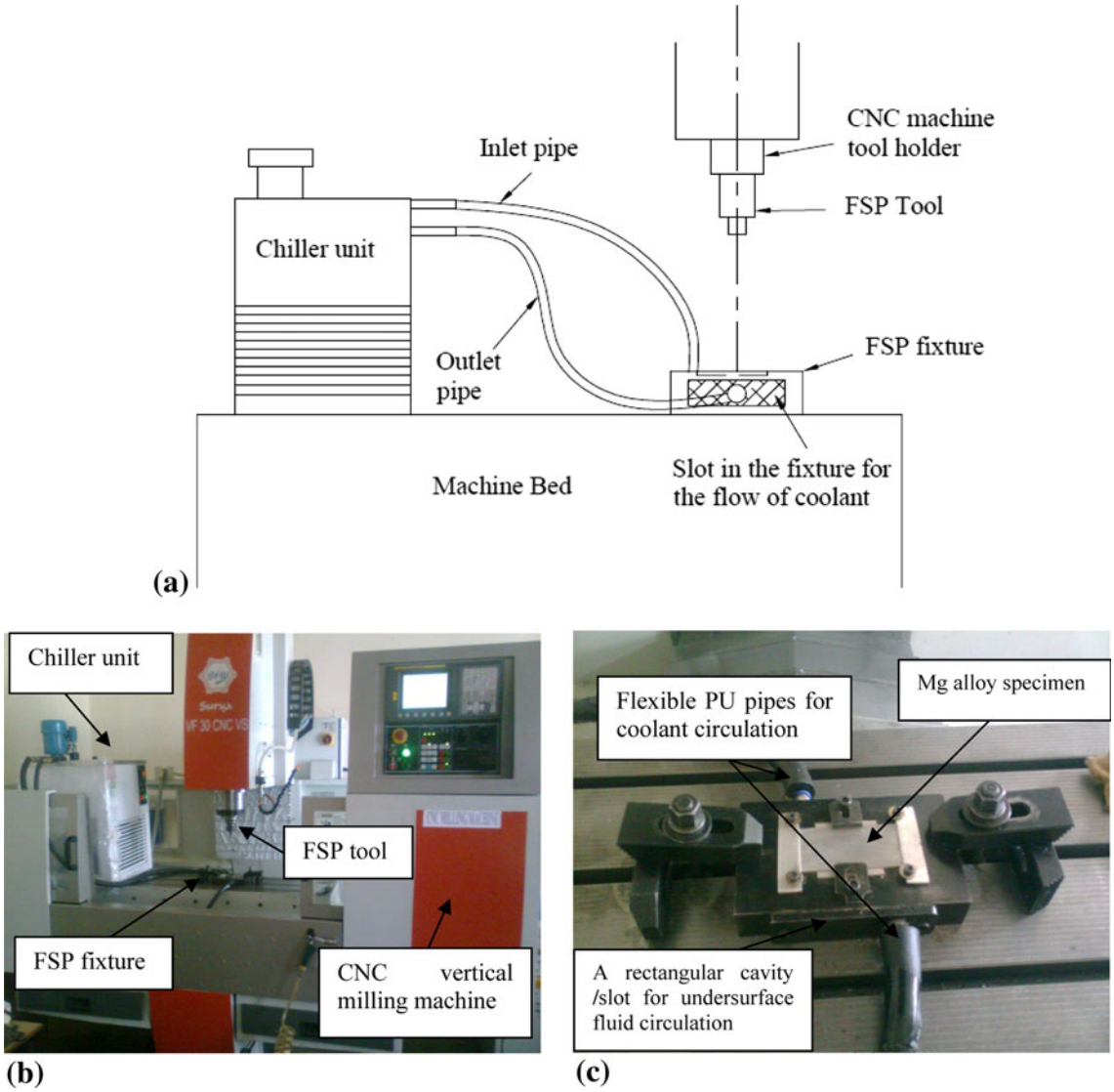

Fig. 3 (a) Schematic of the set-up used in the current investigation (b) and (c). Details of the set-up and the fixture used in the current investigation (Ref 29)

was calculated in all the cases using "larger is better" option which is given as

$$\frac{S}{N}\text{ratio; larger is better} = -10\log_{10}\left[\sum\left(\frac{1}{y^2}\right)\Big/n\right]$$

where y is the output response (the hardness of the FSPed specimen), n is the number of observations. The response table for SN ratios was used to determine the most influencing and the least influencing parameter among the investigated parameters. The rank of the parameters in order of their influence on the output response was also established by the software depending upon their SN ratios. Main effects plots for SN and interaction plot for SN ratios were used to determine the optimum combination of FSP parameters which provides highest value of the output response, the hardness of the FSPed specimen, for the current analysis. Analysis of variance (ANOVA) test results were used to determine the significance of the various factors in terms of their P values at 90% confidence level. The factors having P values <0.1 in the ANOVA test results are considered significant in terms of their influence on the output response, whereas factors having P values >0.1 are considered as statistically insignificant.

3. Results and Discussion

3.1 Most Influencing Process Parameters

The Vickers hardness values of as-cast AE42 and FSPed specimens which is the output response in the current investigation as well as the average grain size values in the different investigated cases is shown in Table 4. The main effects plots of the SN ratios for all investigated parameters are shown in Fig. 5. It is evident from the figure that as the factor level for parameters A, B, and E varies from level 1 to 3, the mean SN ratio changes by noticeable value whereas the change is insignificant for parameters C and D. In other words, it can be said that for the current investigation, parameters A, B, and E

Table 3 Taguchi's L_{27} orthogonal array

Column numbers	1	2	3	4	5	6	7	8	9	10	11	12	13
Exp	*A*	*B*	*A* × *B*		*C*			*A* × *C*	*D*	*E*			
1	1	1	1	1	1	1	1	1	1	1	1	1	1
2	1	1	1	1	2	2	2	2	2	2	2	2	2
3	1	1	1	1	3	3	3	3	3	3	3	3	3
4	1	2	2	2	1	1	1	2	2	2	3	3	3
5	1	2	2	2	5	2	2	3	3	3	1	1	1
6	1	2	2	2	3	3	3	1	1	1	2	2	2
7	1	3	3	3	1	1	1	3	3	3	2	2	2
8	1	3	3	3	2	2	2	1	1	1	3	3	3
9	1	3	3	3	3	3	3	2	2	2	1	1	1
10	2	1	2	3	1	2	3	1	2	3	1	2	3
11	2	1	2	3	2	3	1	2	3	1	2	3	1
12	2	1	2	3	3	1	2	3	1	2	3	1	2
13	2	2	3	1	1	2	3	2	3	1	3	1	2
14	2	2	3	1	2	3	1	3	1	2	1	2	3
15	2	2	3	1	3	1	2	1	2	3	2	3	1
16	2	3	1	2	1	2	3	3	1	2	2	3	1
17	2	3	1	2	2	3	1	1	2	3	3	1	2
18	2	3	1	2	3	1	2	2	3	1	1	2	3
19	3	1	3	2	1	3	2	1	3	2	1	3	2
20	3	1	3	2	2	1	3	2	1	3	2	1	3
21	3	1	3	2	3	2	1	3	2	1	3	2	1
22	3	2	1	3	1	3	2	2	1	3	3	2	1
23	3	2	1	3	2	1	3	3	2	1	1	3	2
24	3	2	1	3	3	2	1	1	3	2	2	1	3
25	3	3	2	1	1	3	2	3	2	1	2	1	3
26	3	3	2	1	2	1	3	1	3	2	3	2	1
27	3	3	2	1	3	2	1	2	1	3	1	3	2

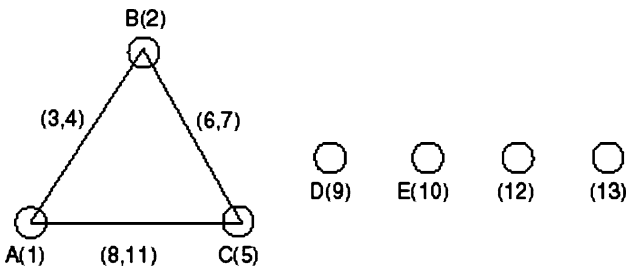

Fig. 4 Line graph for L_{27} orthogonal array

are significant in terms of their influence on output response, whereas factors *C* and *D* are not as significant. The same conclusion is endorsed by ANOVA for mean value results shown in Table 5. Since the analysis was carried out at 90% confidence limit as mentioned earlier also, so the following criteria was used for the determination of significance level of the investigated parameter

for $P > 0.1$; the factor is considered to be insignificant

and

for $P \leq 0.1$; the factor is considered to be significant

The *P* value for parameters *A*, *B*, and *E* is ≤ 0.1 as calculated in Table 5 and hence are statistically significant, whereas the corresponding value for factors *C* and *D* is >0.1 and hence insignificant. From the SN values for different parameters at different levels as shown in Fig. 5, it is predictable that the factor combination of $A_1B_1C_2D_2E_3$ gives highest

Table 4 Actual values of parameters, mean hardness, and average grain size in different experimental runs

Sr. nos.	*A*	*B*	*C*	*D*	*E*	HV	Average grain size, μm
1	700	−10	40	0.25	1	69.4	1.9
2	700	−10	50	0.3	2	71.9	1.25
3	700	−10	60	0.35	3	74.1	1.05
4	700	10	40	0.3	2	67.5	1.55
5	700	10	50	0.35	3	72.2	1.41
6	700	10	60	0.25	1	67.3	2.09
7	700	30	40	0.35	3	62.9	2.52
8	700	30	50	0.25	1	66.6	2.02
9	700	30	60	0.3	2	64.6	2.57
10	800	−10	40	0.3	3	71.0	1.25
11	800	−10	50	0.35	1	65.4	2.10
12	800	−10	60	0.25	2	69.0	1.45
13	800	10	40	0.35	1	65.8	2.95
14	800	10	50	0.25	2	67.6	1.96
15	800	10	60	0.3	3	68.5	1.5
16	800	30	40	0.25	2	62.9	2.72
17	800	30	50	0.3	3	64.2	2.88
18	800	30	60	0.35	1	65.8	2.22
19	900	−10	40	0.35	2	66.6	1.58
20	900	−10	50	0.25	3	69.6	1.47
21	900	−10	60	0.3	1	65.3	2.38
22	900	10	40	0.25	3	68.2	1.98
23	900	10	50	0.3	1	64.9	2.9
24	900	10	60	0.35	2	61.7	3.02
25	900	30	40	0.3	1	65.4	3.97
26	900	30	50	0.35	2	61.3	4.66
27	900	30	60	0.25	3	60.2	5.08
28	As-cast AE42					48	15

hardness of the nugget zone of the FSPed specimen. Since this factor combination is not included in the 27 experimental runs, so the hardness value in this case can be predicted using following equation:

$$\text{Nugget hardness (NH)} = \overline{T} + (\overline{A_1} - \overline{T}) + (\overline{B_1} - \overline{T}) + (\overline{C_2} - \overline{T}) + (\overline{D_2} - \overline{T}) + (\overline{E_3} - \overline{T})$$

where $\overline{T}$ is the mean hardness value, $\overline{A_1}$, $\overline{B_1}$, $\overline{C_2}$, $\overline{D_2}$, and $\overline{E_3}$ represent the mean hardness value of the FSPed specimens when factors *A*, *B*, *C*, *D*, and *E* are, respectively, at levels 1, 1, 2, 2, and 3. These values can be obtained from Table 6 which is the response table for means. Substituting the values in the preceding equation

$$\text{Nugget hardness} = 66.67 + (68.50 - 66.67) + (69.14 - 66.67) + (67.13 - 66.67) + (67.02 - 66.67) + (67.87 - 66.67) = 73\text{HV}$$

Factors *C* and *D* being insignificant, the effective or influencing factor combination for the highest nugget hardness (NH) is $A_1B_1E_3$. This factor combination is the third experimental run in the orthogonal array shown in Table 3, for which the hardness value shown in Table 4, is nearly the same as calculated above. The interaction plot for SN ratios for factors *A* and *B* is shown in Fig. 6. It is perceptible from the figure that factors *A* and *B* have poor interaction with each other as the lines for factor *B* at different levels of factor *A* does not cross or intersect each other.

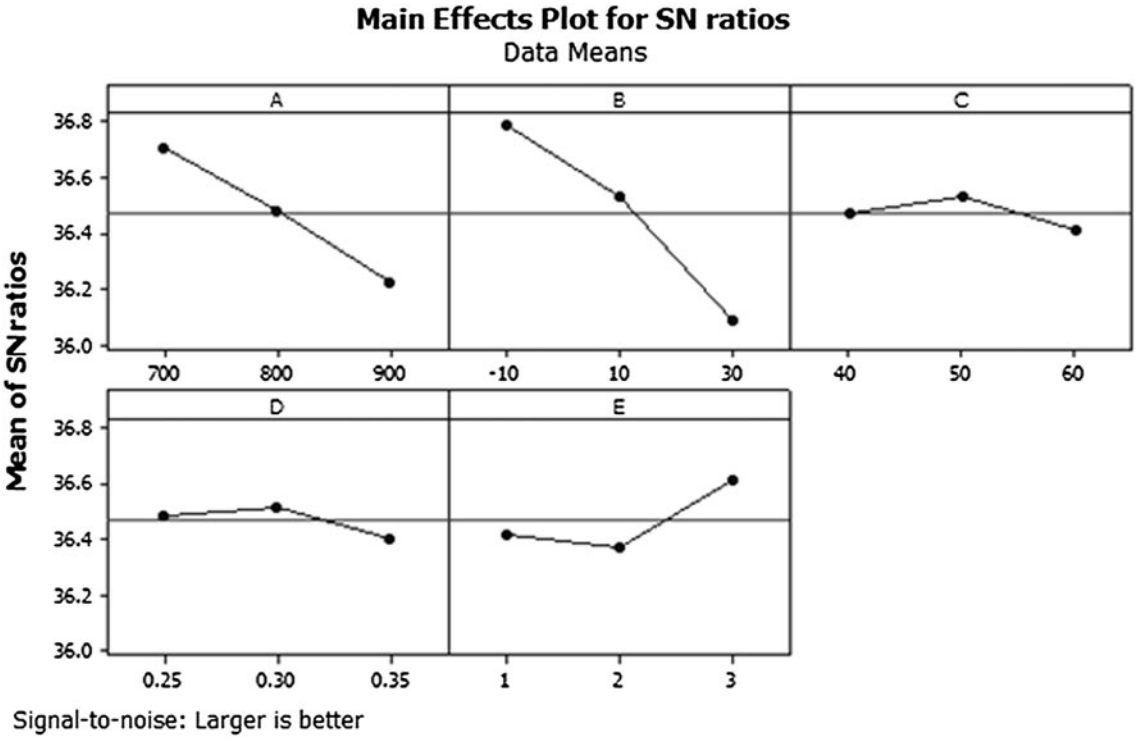

Fig. 5 Main effects plot for SN ratios showing influence of FSP parameters on the hardness value

Table 5 ANOVA for means

Sources	DF	Seq SS	Adj SS	Adj MS	*F*	*P*
A	2	61.647	61.647	30.823	9.25	0.008
B	2	132.809	132.809	66.404	19.93	0.001
C	2	3.407	3.407	1.703	0.51	0.618
D	2	3.282	3.282	1.641	0.49	0.628
E	2	19.376	19.376	9.688	2.95	0.101
$A \times B$	4	7.784	7.784	1.946	0.58	0.683
$A \times C$	4	50.833	50.833	12.708	3.82	0.051
Residual error	8	26.649	26.649	3.331		
Total	26	305.787				

The *P* value for this interaction pair is 0.683(>0.1) as calculated in Table 5 which endorses the fact of the interaction being insignificant for the considered output response and investigated factors. The interaction plot for factors *A* and *C* is shown in Fig. 7. The line for factor *C* at different levels of factor *A* can be seen to cross each other in this figure which indicates that the interaction between this pair is relatively significant which is supported by lower *P* value (0.051) for this interacting pair as calculated in Table 5. The mean hardness values at different parameter levels have been calculated and are shown in Table 6. The "delta" value shown in this table was calculated for each parameter from the difference of the maximum mean hardness value and minimum mean hardness value at different levels. The rank of each parameter was determined from the delta values of all the parameters as shown in Table 6. The rank of the parameters signifies their relative importance in terms of their influence on the output response, i.e., hardness values in this investigation. Cooling temperature, parameter *B*, was found to be most influential parameter among the investigated ones.

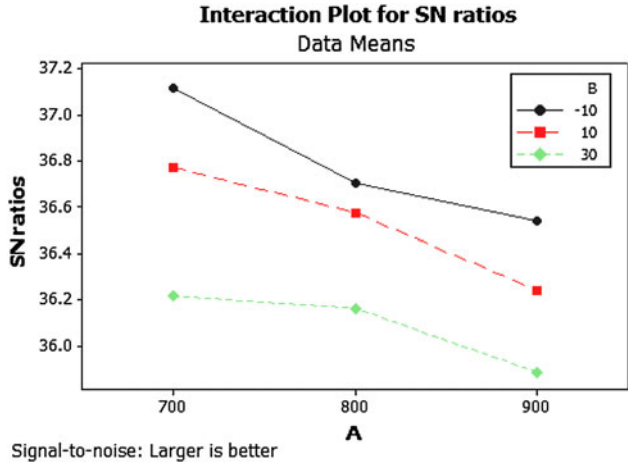

Fig. 6 Interaction plot between $A \times B$ for the hardness value

The 3-D surface plots showing the variation of hardness (HV) of FSPed AE42 alloy with respect to the influential FSP parameters namely tool rpm, cooling temperature, and number of FSP passes are shown in Fig. 8 to 10.

Chang et al. (Ref 27) have investigated the influence of cooling rate on the microstructure evolution and hardness of the FSPed AZ31 magnesium alloy. In their investigation, they found that there was a tremendous increase in the hardness of the FSPed specimen with high cooling rates where it increased nearly three folds than that of the base material. Thus, the finding of cooling rate being an extremely important parameter during FSP, influencing the mechanical property of the FSPed specimen agrees well with the findings of other investigators.

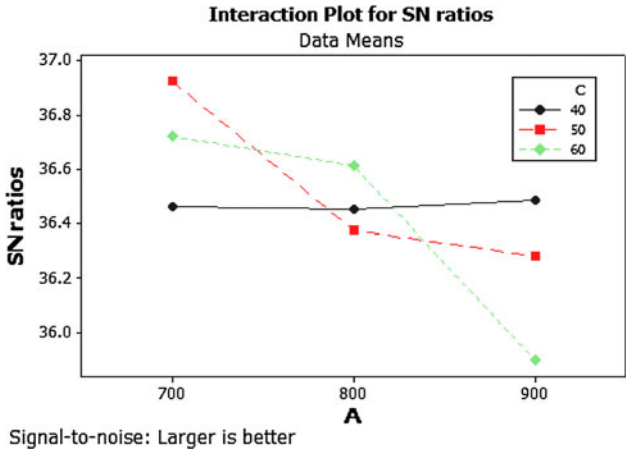

Fig. 7 Interaction plot between $A \times C$ for the hardness value

Table 6 Response table for means

Levels	*A*	*B*	*C*	*D*	*E*
1	68.50	69.14	66.63	66.81	66.21
2	66.73	67.12	67.13	67.02	65.96
3	64.80	63.77	66.27	66.20	67.87
Delta	3.70	5.38	0.87	0.82	1.91
Rank	2	1	4	5	3

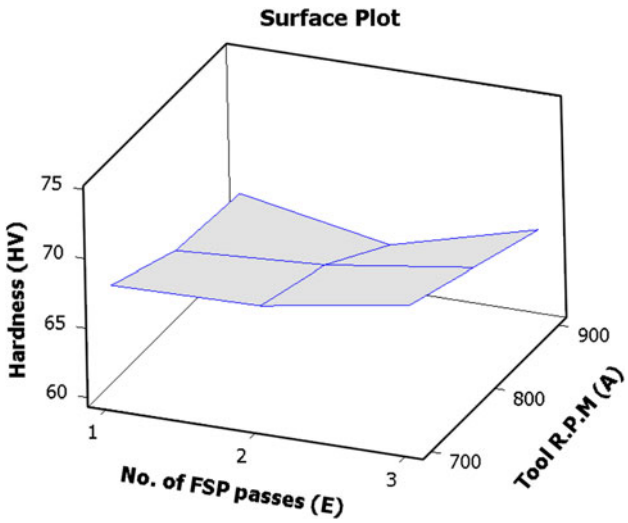

Fig. 8 3-D surface plot showing HV with respect to tool rpm (parameter *A*) and number of FSP passes (parameter *E*) for the FSPed AE42 alloy

3.2 Effect of Different Process Parameters

As discussed above, the most influential FSP process parameters at 90% confidence limit for the range of parameters and factors investigated were found to be FSP tool rpm, cooling temperature during FSP, and number of FSP passes. Therefore, the observed behavior of FSP AE42 has been explained in terms of these parameters. The optical images of as-cast AE42 alloy and for some of the selected cases of FSP AE42 corresponding to the 3rd, 7th 13th and 27th rows in Table 4 are shown in Fig. 11 and the average grain size values in all the

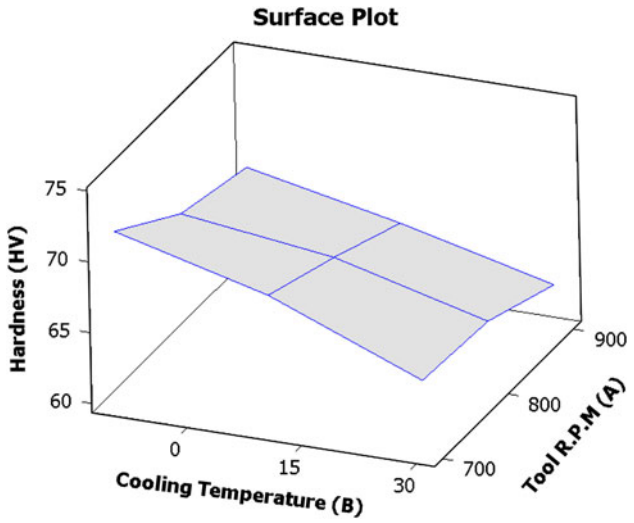

Fig. 9 3-D surface plot showing HV with respect to tool rpm (parameter *A*) and cooling temperature (parameter *B*) for the FSPed AE42 alloy

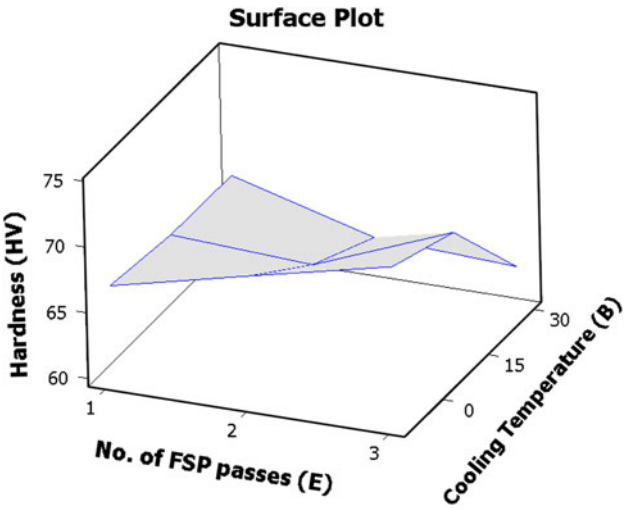

Fig. 10 3-D surface plot showing HV with respect to cooling temperature (parameter *B*) and number of FSP passes (parameter *E*) for the FSPed AE42 alloy

investigated cases are shown in Table 4. It is evident from the average grain size values that grain size got considerably refined after FSP at all the process parameters with the corresponding increase in the average hardness values as compared to the as-cast AE42 alloy; however, the extent of grain refinement depends on the factor levels. This observed behavior can be explained using well-known Hall-Petch equation given by the following equation:

$$\sigma_0 = \sigma_i + kD^{-1/2}$$

where σ_0 is the yield stress, σ_i is the "friction stress," representing the overall resistance of the crystal lattice to dislocation movement, k is the "locking parameter," which measures the relative hardening contribution of the grain boundaries, and D is the grain diameter. The equation states that the hardness value is inversely proportional to the grain size. Thus, in accordance with the above equation, as the grain diameter/grain size decreases, the yield strength, as well

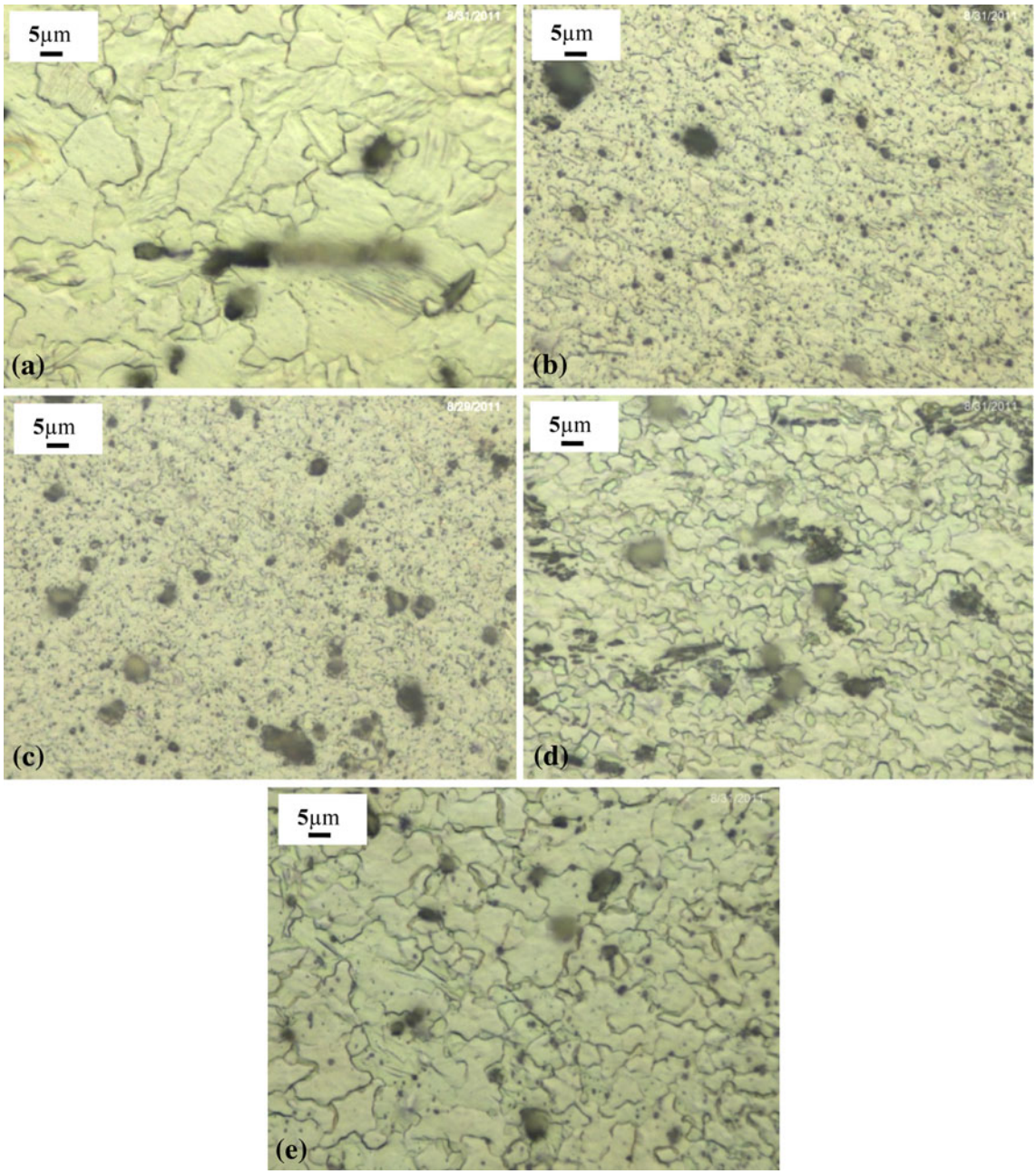

Fig. 11 Optical images of (a) as-cast AE42, (b) to (e) FSP AE42 at different process conditions corresponding to the 3rd, 7th 13th, 27th rows in Table 4 showing the grain size in the different cases

as, the hardness of the material increases. In the previous investigation by the authors (Ref 29), it was found that two strengthening phenomenon which were responsible for enhancing the strength of the FSP AE42 alloy were grain size strengthening and Orowan strengthening. However, the major contributing phenomena was found to be grain size strengthening, whereas Orowan strengthening was found to contribute only marginally. Grain size strengthening contributes towards improved material performance in accordance with the Hall-Petch equation. The in-situ particles have largely contributed towards evolution of finer grain structure by the way of pinning effect. This effect could also be represented in the Hall-Petch equation only. Thus, the enhanced hardness of the FSP AE42 alloy may be attributed to the appearance of fine grain structure. Further, it can be observed from Table 4 that the grain size refinement and the corresponding rise in the hardness values of multipass FSP AE42 at constant cooling temperatures of −10 °C (263 K) and 10 °C (283 K) (parameter *B*) is higher than the single pass FSP AE42 at all other FSP process parameters. The possible reason for this behavior may be attributed to the presence of fine precipitate particles generated in situ in the AE42 alloy during multipass FSP, which get accumulated near the fine nuclei formed during dynamic recrystallization (DDRX) and pin them, the details of which are given elsewhere (Ref 29). Along with the grain boundary pinning by fine precipitate particles, rapid cooling rates further aid in the evolution of fine grain structure by restricting the time and energy available for the growth of

recrystallized nuclei. However, it can be observed that the grain structure became coarser and the corresponding hardness values decreased with multipass FSP at higher cooling temperature of 30 °C. It is believed that in this case also the presence of fine precipitate particles (Ref 29) contribute in the evolution of fine grain structure but slower cooling rates provided more time for the growth of recrystallized fine nuclei and thus resulted in comparatively coarser grain structure. Increase in the average grain size values with the corresponding decrease in hardness values at 800 and 900 tool rpm at the same cooling temperature can also be observed from Table 4. The major part of the heat generation in the FSP process is the frictional heat by the FSP tool shoulder. Therefore, FSP tool rpm is one of the key parameters which decide the amount of heat input into the FSPed zone. Mishra and Ma (Ref 28) had shown that higher the FSP tool rpm, higher will be the heat input. Thus, higher heat content at higher tool rpm resulted in longer cooling times at the same cooling temperature and a comparatively coarser grain structure. This observed behavior highlights the significance of higher cooling rates, optimum tool rpm, and the number of FSP passes.

Linear speed is another parameter that affects the heat input into the FSP zone. Whereas linear speed decides the length of exposure of FSP zone to the heat, the tool rpm is one of the factors which decide the magnitude of the heat content. In accordance with Mishra and Ma (Ref 28), higher tool rpm results in higher heat input whereas higher tool linear speed results in lower heat input. Therefore, the amount of heat input in the FSP zone at some level of factor A (tool rpm) also depends on the level of factor C (linear speed) at the same level of factor A. In other words, factors A and C interact with each other. This is supported by considerably low P value (0.051) of the interaction term $A \times C$ in the ANOVA table (Table 5). On the other hand, the effect of tool rpm (factor A) at any level does not appear to depend on the level of factor B (cooling temperature) as indicated by comparatively high P value (0.683) of the interaction term $A \times B$ in the ANOVA table. It has been reported by Yazdipour et al. (Ref 31) that the amount of heat input into the stir zone affects the nuclei size and the nucleation mechanism, whereas the cooling rate does not influence it. However, the cooling rate during FSP affects the growth rate of the fine nuclei formed during the recrystallization process. As discussed earlier, FSP tool rpm is one of the important parameters that determine the amount of heat input. Thus, it is believed that the tool rpm affects the nuclei size formed during FSP, whereas cooling rate influences its growth rate only. It can thus be concluded that although both the tool rpm and the cooling rate affects the overall grain refinement and mechanical properties of the material, but the performance of one parameter does not depend on the level of other. In other words, these parameters do not interact with each other.

3.3 Developing Empirical Relationship

The results of the ANOVA analysis revealed that only three factors namely FSP tool rpm (factor A), cooling temperature (factor B), and number of FSP passes (factor E) have significant influence on the hardness of the FSPed specimens. Thus, it can be concluded that hardness of the FSPed specimen in the current investigation is the function of the above-listed parameters and it can be expressed as

$$\text{Nugget hardness (NH)} = f(A, B, E)$$

For conducting nonlinear regression analysis, the polynomial equation can be expressed as

$$\begin{aligned}\text{Nugget hardness (NH)} = {} & C_1 + C_2A + C_3B + C_4E + C_5A^2 \\ & + C_6B^2 + C_7E^2 + C_8AB + C_9AE \\ & + C_{10}BE + C_{11}ABE\end{aligned}$$

where $C_1, C_2, C_3, C_4, C_5, C_6, C_7, C_8, C_9, C_{10}$, and C_{11} are the constants whose values depend on the main and interaction effects of the parameters on the output response. The above polynomial equation was developed for the current investigation using nonlinear regression on MINITAB 16 software. The analysis was conducted at 95% confidence limit. The equation was built in the software after 200 iterations using Gauss Newton algorithm of least square technique and the resultant equation is given as

$$\begin{aligned}\text{Nugget hardness (HV)(HV)} = {} & 76.35 - 0.0035A - 0.225B \\ & - 0.676E - 8.333e-006A^2 \\ & - 0.001667B^2 + 1.0833E^2 \\ & + 0.0004166AB - 0.00222AE \\ & - 0.0495BE - 6.875e-005ABE\end{aligned}$$

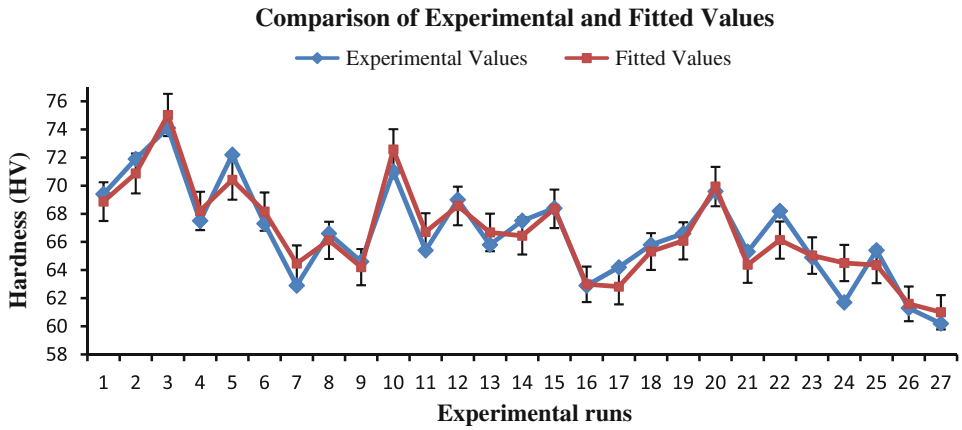

Fig. 12 Comparison between experimental and fitted hardness values for the 27 experimental runs. The *error bars* are shown at 2% magnitude

3.4 Adequacy Checking of the Developed Model

The adequacy of the developed empirical model was tested using

1. Comparison of the experimental hardness values with that of the predicted ones and calculating the resultant error.
2. Residual plots of the NH.

The experimental hardness values obtained in the different investigated cases and the corresponding values obtained from the developed nonlinear regression equation have been compared in Fig. 12. It can be seen that the predicted hardness values from the developed model are very close to the experimental values in most of the experimental runs. The error between the experimental and the predicted values has been shown in the figure in terms of error bars at magnitude of 2%. The magnitude of error in most of the predicted values is $<1\%$. FSPed specimen at some other parameter combinations which were not included in the investigated 27 experimental runs was also used for the evaluation of the proposed model. The parameter combinations, experimental hardness values, hardness values predicted by the developed model as well as corresponding percentage error in the predicted values are shown in Table 7. As evident from the table, the developed model accurately predicts the hardness values with magnitude of error $<1\%$ in most of the experimental runs. The residual plots of the developed model for the NH as shown in Fig. 13 highlight similar results as obtained from the comparison of experimental and the predicted values. In normal probability plot, with the exception of few values, the residuals can be seen to lie very close to the mean line. Approximately same number of data points can be seen to fall on the either side of the zero residual line in the plot for fits. The histogram shown in the figure depicts a nearly normal distribution curve for the residuals. These results indicate that the proposed equation is statistically significant and endorse the suitability of the proposed model.

Table 7 Predicted and experimental hardness values for different parameter combinations

Sr. nos.	Parameter combination	Predicted HV from regression equation	Actual experimental HV	Percentage error
1	$A_3B_1C_3D_2E_2$	65.42	66.2	1.1
2	$A_3B_3C_3D_2E_2$	63.00	61.2	2.9
3	$A_3B_3C_3D_2E_1$	63.96	63.5	0.7
4	$A_2B_3C_3D_2E_2$	63.06	62.7	0.5
5	$A_2B_1C_3C_2E_2$	67.44	68.3	1.25

4. Summary and Conclusions

A systematic evaluation of the FSP parameters, namely rotational speed, cooling temperature, linear speed, plunge depth and number of FSP passes, has been presented using Taguchi's experimental design technique to determine the optimum combination of FSP parameters and their levels among the selected ones. Cooling temperature during FSP, FSP tool rotational speed, and number of FSP passes were found to be the most influential FSP parameters. Cooling temperature during FSP and thus cooling rate significantly affect the grain growth rate and the final grain size of the FSPed specimen. The finer grain size produced with the application of higher cooling

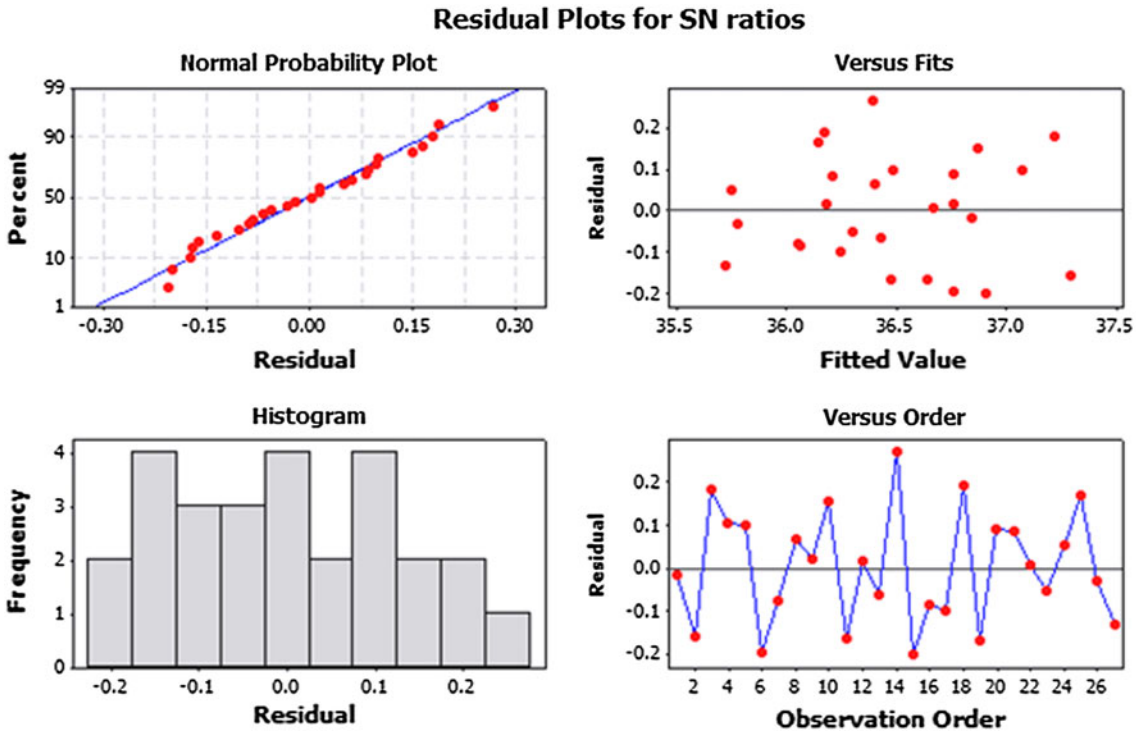

Fig. 13 Residuals plots for the NH values predicted using nonlinear regression model

rate during FSP enhances the material strength in accordance with the well-known Hall-Petch equation. Further, FSP tool rotational speed plastically deforms the material by imposing strain and strain rate gradients. FSP tool rpm also affects the degree of precipitate/particle refinement produced in the material. However, higher tool rpm exposes the specimen to higher temperatures which adversely affects the grain size of the FSPed material. Number of FSP passes is another significant parameter which affects the precipitate/particle refinement. In general, higher number of FSP passes can produce finer particle/precipitate size which enhances the material strength through particle pinning phenomena. Thus, the Taguchi's experimental design technique contributed significantly in selecting the optimum parameters for the FSP technique as well as provides directions toward the possible mechanisms behind the process which otherwise is a complex task with the usual experimentation and analysis techniques.

The results of this investigation can be summarized as

1. Optimized FSP parameters were obtained for AE42 magnesium alloy using Taguchi's experimental design approach where hardness of the FSPed specimen was utilized as the output response.
2. The selected range of parameters for defect free FSP zone is believed to be valid for the investigated magnesium alloy AE42 and they may be different for other magnesium alloys.
3. FSP tool rpm, cooling temperature during FSP, and number of FSP passes were found as influential parameters at 90% confidence limit. Cooling temperature was found to be the most influential parameter affecting the hardness of the nugget zone of FSPed specimen while plunge depth of the FSP tool was found to be least influential.
4. Empirical relationship was developed for the hardness of the nugget zone of the FSPed specimen in terms of the FSP parameters using a nonlinear regression equation. The nonlinear equation developed is a system specific equation. It is believed to be valid for AE42 magnesium alloy within the range of parameters and their levels chosen.
5. The developed empirical relation was observed to accurately predict the hardness of the FSPed specimen within the range of FSP parameters chosen.

References

1. G.V. Raynor, *The Physical Metallurgy of Magnesium and its Alloys*, Pergamon Press, Amsterdam, 1959, p 254
2. R.W. Cahn, P. Haasan, and E.J. Kramer, *Material Science Technology*, Vol 8, VCH-Verlagsgesellschaft, Weinheim, 1996
3. Z. Liu and W. Gao, Electroless Nickel Plating on AZ91Mg Alloy Substrate, *Surf. Coat. Technol.*, 2006, **200**, p 5087–5093
4. P.J. Blau and M. Walukas, Sliding Friction and Wear of Magnesium Alloy AZ91D Produced by Two Different Methods, *Tribol. Int.*, 2000, **33**, p 573–579
5. H. Hoche, C. Rosenkranz, A. Delp, M.M. Lohrengel, E. Broszeit, and C. Berger, Investigation of the Macroscopic and Microscopic Electrochemical Corrosion Behaviour of PVD-Coated Magnesium Die Cast Alloy AZ91, *Surf. Coat. Technol.*, 2005, **193**(1–3), p 178–184
6. S.K. Wu, S.C. Yen, and T.S. Chou, A Study of r.f.-Sputtered Al and Ni Thin Films on AZ91D Magnesium Alloy, *Surf. Coat. Technol.*, 2006, **200**, p 2769–2774
7. S.K. Thakur, B.K. Dhindaw, N. Hort, and K.U. Kainer, Some Studies on the Thermal-Expansion Behavior of C-Fiber, SiCp, and In-Situ Mg_2Si-Reinforced AZ31Mg Alloy-Based Hybrid Composites, *Metall. Mater. Trans. A*, 2004, **35A**, p 1167–1176
8. S. Ugandhar, M. Gupta, and S.K. Sinha, Enhancing Strength and Ductility of Mg/SiC Composites Using Recrystallization Heat Treatment, *Compos. Struct.*, 2006, **72**, p 266–272
9. A. Arunachaleswaran, I.M. Pereira, H. Dieringa, Y. Huang, N. Hort, B.K. Dhindaw, and K.U. Kainer, Creep Behavior of AE42 Based Hybrid Composites, *Mater. Sci. Eng., A*, 2007, **461**, p 268–276
10. D.U. XingHao and W.U. BaoLin, Using Two-Pass Friction Stir Processing to Produce Nanocrystalline Microstructure in AZ61 Magnesium Alloy, *Sci China E*, 2009, **52**(6), p 1751–1755
11. R.S. Mishra and M.W. Mahoney, Friction Stir Processing: A New Grain Refinement Technique to Achieve High Strain Rate Superplasticity in Commercial Alloys, *Mater. Sci. Forum*, 2001, **357**(3), p 507–512
12. R.S. Mishra, M.W. Mahoney, and S.X. McFadden, High Strain Rate Superplasticity in a Friction Stir Processed 7075 Al Alloy, *Scripta Mater.*, 2000, **42**, p 163–168
13. S. Benavides, Y. Li, and L.E. Murr, Ultrafine Grain Structure in the Friction-Stir Welding of Aluminium Alloy 2024 at Low Temperatures, *Proceedings of Ultrafined Grained Materials, TMS*, 2000, p 155–168
14. N. Saito, I. Shigematsu, and T. Komaya, Grain Refinement of 1050 Aluminum Alloy by Friction Stir Processing, *J. Mater. Sci. Lett.*, 2001, **20**, p 1913–1915
15. Y.J. Kwon, N. Saito, and I. Shigematsu, Friction Stir Process as a New Manufacturing Technique of Ultrafine Grained Aluminum Alloy, *J. Mater. Sci. Lett.*, 2002, **21**, p 1473–1476
16. T.A. Freeney and R.S. Mishra, Effect of Friction Stir Processing on Microstructure and Mechanical Properties of a Cast Magnesium Rare Earth Alloy, *Metall. Mater. Trans. A*, 2010, **41**, p 73–84
17. D.R. Ni, D. Wang, A.H. Feng, G. Yao, and Z.Y. Ma, Enhancing the High-Cycle Fatigue Strength of Mg-9Al-1Zn Casting by Friction Stir Processing, *Scripta Mater.*, 2009, **61**, p 568–571
18. P. Cavaliere and P.P. DeMarco, Superplastic Behaviour of Friction Stir Processed AZ91 Magnesium Alloy Produced by High Pressure Die Cast, *J. Mater. Process. Technol.*, 2007, **184**, p 77–83
19. W. Yuan, R.S. Mishra, B. Carlson, R.K. Mishra, R. Verma, and R. Kubic, Effect of Texture on the Mechanical Behavior of Ultrafine Grained Magnesium Alloy, *Scripta Mater.*, 2011, **64**, p 580–583
20. R.S. Mishra and M.W. Mahoney, *Friction Stir Welding and Processing*, ASM International, Materials Park, 2007
21. Y.C. Chen, H. Liu, and J. Feng, Friction Stir Welding Characteristics of Different Heat-Treated-State 2219 Aluminium Alloy Plates, *Mater. Sci. Eng., A*, 2006, **420**(1–2), p 21–25
22. K. Elangovan, V. Balasubramanian, and M. Valliappan, Influences of Tool Pin Profile and Axial Force on the Formation of Friction Stir Processing Zone in AA6061 Aluminium Alloy, *Int. J. Adv. Manuf. Technol.*, 2008, **38**, p 285–295
23. L. Karthikeyan, V.S. Senthilkumar, and K.A. Padmanabhan, On the Role of Process Variables in the Friction Stir Processing of Cast Aluminum A319 Alloy, *Mater. Des.*, 2010, **31**, p 761–771
24. C.F. Chen, P.W. Kao, L.W. Chang, and N.J. Ho, Effect of Processing Parameters on Microstructure and Mechanical Properties of an Al-$Al_{11}Ce_3$-Al_2O_3 In-Situ Composite Produced by Friction Stir Processing, *Metall. Mater. Trans. A*, 2010, **41a**, p 513–522
25. P. Cavaliere, A. Squillace, and F. Panella, Effect of Welding Parameters on Mechanical and Microstructural Properties of AA6082 Joints Produced by Friction Stir Welding, *J. Mater. Process. Technol.*, 2008, **200**, p 364–372
26. C.I. Chang, X.H. Du, and J.C. Huang, Achieving Ultrafine Grain Size in Mg-Al-Zn Alloy by Friction Stir Processing, *Scripta Mater.*, 2007, **57**, p 209–212
27. C.I. Chang, X.H. Du, and J.C. Huang, Producing Nanograined Microstructure in Mg-Al-Zn Alloy by Two-Step Friction Stir Processing, *Scripta Mater.*, 2008, **59**, p 356–359
28. R.S. Mishra and Z.Y. Ma, Friction Stir Welding and Processing, *Mater. Sci. Eng. R*, 2005, **50**, p 1–78
29. H.S. Arora, H. Singh, and B.K Dhindaw, Some Observations on Microstructural Changes in a Mg-Based AE42 Alloy Subjected to Friction Stir Processing, *Metall. Mater. Trans. B*, 2011. doi:10.1007/s11663-011-9573-7
30. R. Roy, *Designs with Interactions, A primer on Taguchi Method*, Van Nostrand Reinhold, New York, 1990, p 61
31. A. Yazdipoura, A. Shafiei, and K. Dehghani, Modeling the Microstructural Evolution and Effect of Cooling Rate on the Nanograins Formed During the Friction Stir Processing of Al5083, *Mater. Sci. Eng., A*, 2009, **527**, p 192–197